

Report: On the activities of the 1st year of PhD

PhD Title- Single Photons On-Demand from a 2D Material Heterostructure.

Student:

Tiago Queirós

Supervisors:

Dr. rer. nat. Jana B. Nieder, INL- International Iberian Nanotechnology Laboratory in Braga, Portugal .

Prof. Dr. Pedro Alpuim, Department of Physics, U Minho and INL

Contents

Preamble.....	3
Introduction.....	3
WP0: Academic Programme.....	4
WP1: Fabrication of hBN, Graphene and hybrid devices	5
WP1.1. Materials.....	5
-WP1.1.1. Material growth.....	5
WP1.2. Devices	7
-WP1.2.1. Designs for 2D material heterostructure devices.....	7
-WP1.2.2. Processes for fabrication	9
WP2: Graphene and hBN Material characterization	12
-WP2.1. Morphological characterization.....	12
-WP2.2. Material quality characterization.....	14
-WP2.3. Single emitter characterization using Widefield TIRF Microscopy	14
-WP2.4. Single emitter characterization using lambda mode confocal fluorescence Microscopy	15
WP3: Development of new methodologies for SPE data analysis.....	16
-WP3.1. Protocols for analysis of Widefield TIRF recordings.....	17
-WP3.2. Protocols for spectral analysis and extraction of useful data from confocal fluorescence microscopy hyperspectral data sets.....	20
Results.....	21
-Graphene properties.....	21
-Density of defects in hBN	22
-Advanced hBN SPE spectra characteristics and intermittency behaviour.....	23
Conclusions:.....	30
Collaborations.....	31
Dissemination.....	32
Participation in seminars and conferences:.....	33
References:.....	33

Preamble

In this report, the progress accomplished in the first year of the PhD academic programme and the research project will be described. The report was structured in accent to a research plan and communicates the advances made on the tasks of material growth and characterization and fabrication of a controllable single photon emitter device.

Introduction

Single photon emitters (SPEs) are shaping up to be one of the primary building blocks of future photonic technologies, as this fundamental resource would enable scalable fabrication of quantum information technologies. A perfect on-demand SPE should be capable of emitting singular photons with precision in time, which are indistinguishable amongst each other. This would make possible the implementation of several Quantum technologies such as Quantum computing schemes, Quantum secure communication protocols, and Quantum sensing and metrology¹. SPEs are also often referred to as antibunched light sources, meaning that the light produced by said source follows sub-Poissonian statistics and is distinctly non-classical.

Graphene is a two-dimensional semi-metal whose Fermi level, and thus optical conductivity, can be altered in a myriad of ways, such as electrostatic gating, chemical doping, physical straining, etc². By elevating or lowering the graphene's Fermi level, it is possible to manipulate its properties so it can be control the passage of light via **Pauli blocking**³, which consists in filling all the states in graphene up to a given energy level such that photoelectric transitions can no longer occur for photon energies inferior to the Fermi level.

The complementary crystal lattice matching between graphene and hBN⁴ alongside graphene's light-switching capabilities may prove to be a **highly scalable** means of producing single photon on-demand devices.

In this report, the progress accomplished in the first year of research on the topic of single photons on-demand from a 2D material heterostructure is highlighted. Topics such as chemical vapour deposition of 2D materials, 2D material characterization, fluorescence microscopy and probing of properties of single photon emitter (SPE) in hBN, as well as microfabrication of electrically controllable 2D material SPE platforms are addressed.

WP0: Academic Programme

The MAPfis doctoral programme in physics includes an academic curricular component that featured the following classes and seminars:

The following course elements are part of the Advanced Physics Topics I and will contribute to 12 ECTS points.

-Introduction to Nano-Optics: A tutorials based class where the student is tasked with writing and presenting a report on a Nano-Optics theme of their choosing. In this case the report was on the theme of how to bypass the optical diffraction limit of light using sub-wavelength light-matter interaction;

-Advanced Material Preparation and Characterization: A series of classes on sample preparation and characterization techniques such as sputtering, laser ablation, spectroscopic ellipsometry, Raman spectroscopy, x-ray diffraction, etc... The student was tasked with completing a written test about the subjects covered in the classes and writing a report on one of the techniques explained in the classes (in the case of this student the selected technique was Raman spectroscopy);

-Integration of Single-Photon Sources in Photonic Devices for Quantum Technologies: A tutorials based class requested by the student, as it pertains directly to his PhD topic. The student was tasked to conduct experiments with 2D material chemical vapour deposition and performing image processing analysis for the extraction and characterization of single photon emitter time traces from hBN samples. A report based on the findings was delivered;

-Physics of Electronic Materials and Devices: A series of classes on semiconductor and condensed matter physics and some of its respective applications. The student was tasked to solve homework exercises on the subject.

-Communicating Science: A set of classes on how to prepare, train, and successfully deliver an oral presentation. The student was tasked with delivering a presentation explaining and introducing his PhD topic to a non-scientific audience in the restricted time frame of 3 minutes; (3 ECTS)

-Entrepreneurship: A series of classes introducing entrepreneurship methods and concepts on how to develop and evaluate a business plan. The student was tasked with brainstorming a business idea in a group and developing the business plan for the respective idea. A report, an oral presentation, and an analysis on an article pertaining to the topic of regional development was delivered; (3 ECTS)

-Defence of the Essay: A literature review of the state-of-the-art and introduction to the PhD topic as well as an elaboration and justification of a work plan for the tasks to be undertaken during the PhD were reported. In addition, the essay was defended publicly in an oral presentation before a committee of MAPfis professors. (12 ECTS)

The academic program requires 30 approved ECTS points, thus, the candidate successfully achieved the academic requirements during the first year.

[WP1: Fabrication of hBN, Graphene and hybrid devices](#)

As indicated in the work plan delivered one year prior the first task consisted on the growth and preparation of the 2D materials necessary for the assembly of the 2D material heterostructure.

In the following the progress on these tasks will be described.

[WP1.1. Materials](#)

[-WP1.1.1. Material growth](#)

Continuous **hBN thin films** were prepared by **atmosphere pressure chemical vapour deposition (AP-CVD)**. Firstly, the catalytic substrates used in the growth process

(99.99999% pure 2 by 10 cm² copper foil) were prepared by 1 minute chemical polishing in ultrasounds using a mixture of 10 mL of HCl (37%), 10 mL of FeCl₃, and 280 mL of pure water. The substrates were mounted on a silicon oxide/silicon holder and placed in a quartz tube, centred on the reaction furnace that surrounds the part of the tube where the growth reaction happens. Solid ammonia borane precursor (8.5 mg) is placed in an aluminium crucible which is also mounted in the quartz tube part surrounded by a heater. Secondly, a flow of 100 sccm of Ar/H₂ (95%/5%) gas mixture is injected from one side of the tube for 20 minutes to purge the atmosphere of other potentially reactive gases, like oxygen. Then the substrate is annealed at 1020 °C for 40 minutes, taking the furnace 25 extra minutes to reach this temperature. Post-annealing, the substrate is cooled down to room temperature before the next step, which consists in heating the precursor at 100 °C for 150 minutes under a lower 5 sccm gas flow to sublime the ammonia borane into gas precursors. After triggering the precursor's phase change, the furnace is once more heated to 1020 °C and a gas mixture flow of 100 sccm is injected to act as a carrier gas to the sublimated precursor, which will transport the reagents to the substrate where the hBN growth takes place over the course of 30 minutes after a 25 minute heating step.

Hexagonal Boron Nitride is highly regarded for being a host material for **room temperature** single photon emitters (SPEs)^{5,6}. In line with the objective of assembling a 2D material heterostructure, graphene as transferred onto hBN to study the effects on the emission characteristics on the SPEs.

Graphene flakes and continuous graphene films were grown by **oxygen assisted low pressure chemical vapour deposition (LP-CVD)**. The 5 by 5 and 10 x 10 cm² copper foil substrates were treated with the same chemical polishing treatment as for the hBN growth process and were also oxidised on a hot plate at 250 °C for 30 minutes, to increase the oxygen concentration during growth. This substrate is mounted in a graphite box with a sapphire mounted over it with using two graphite supports. The purpose of the sapphire is to continuously release oxygen during the reaction process which mediates the growth of large graphene crystals. The purpose of the graphite box is to fold, it both confines the atmosphere near the sample to increase the oxygen concentration near the sample and protects the material from the deposition of silicates originating from the sublimation of the quartz tube reactor⁷. The copper foils annealed in an argon atmosphere for 30 minutes at 1040 °C. Methane is injected as a precursor gas

for graphene, along with argon to adjust the partial pressure of the reagents, and hydrogen which mediates the growth process in conjunction with the oxygen to enable the deposition of large crystals and large grain continuous graphene. The grow process is done at 1040 °C. Parameters such as methane, argon, and hydrogen flow, as well as growth time and process pressure were varied to analyse their effects on the sample quality.

In conclusion the growth of the hBN and Graphene material was executed in line with the time plan proposed (First 8 months), and it should be highlighted that a considerably fast speed of fabrication of 30 min for over 1 mm sized graphene flakes was achieved⁸. The quality was enough to perform characterization of functional properties described in WP2.

WP1.2. Devices

-WP1.2.1. Designs for 2D material heterostructure devices

Three strategies were implemented in an effort to assemble electrically addressable 2D material heterostructures for the controlled quantum emission of hBN fluorescent crystal defects. The **first** attempt, illustrated in Figure 1, consisted of a simple manual stacking of graphene, hBN, and graphene layers, where each graphene layer acted as a condenser plate which could be addressed using probe needles and the hBN layer served as the dielectric.

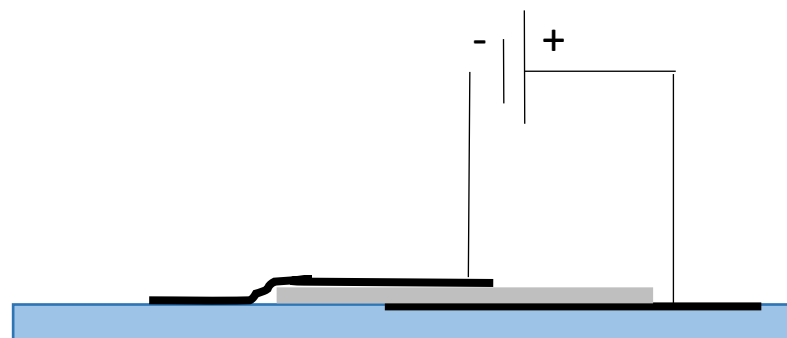


Figure 1: Illustration of the manually assembled stack of 2D materials. The black lines illustrate graphene and the grey layer illustrates the hBN containing SPEs

The **second** strategy involved microfabrication to assemble metal contacts which would facilitate ohmic contact to the graphene layers without damaging the 2D materials and patterning of the heterostructure into 7 by 5 mm² areas.

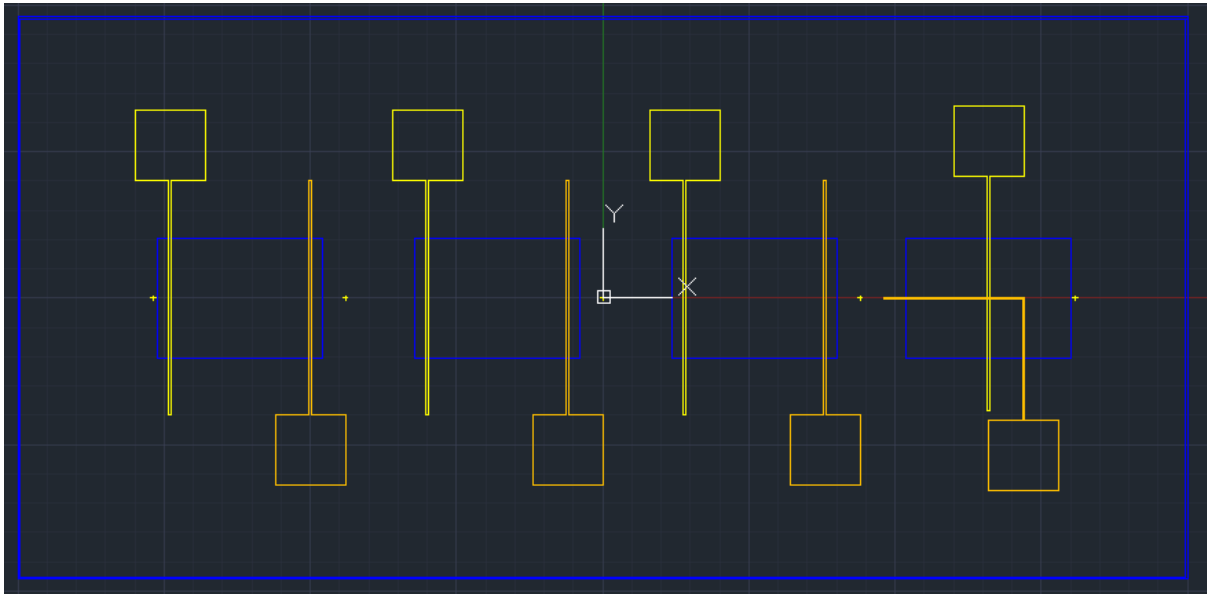


Figure 2: Schematic of the lithography masks used in the devices' microfabrication. The yellow layer represents the metal contacts addressing the bottom graphene layer, the blue rectangles represent the 2D material heterostructure etch protection mask, and the orange mask represents the metal contacts addressing the top graphene layer.

The **third** strategy consisted in replicating the previous process, but with microscopic sized heterostructures and some variety in the design, such as 150 by 150 μm^2 graphene/ hBN/ graphene heterojunctions, 100 by 100 μm^2 graphene/ hBN/ graphene heterojunctions, and 150 by 150 μm^2 gold/ hBN/ graphene heterojunctions.

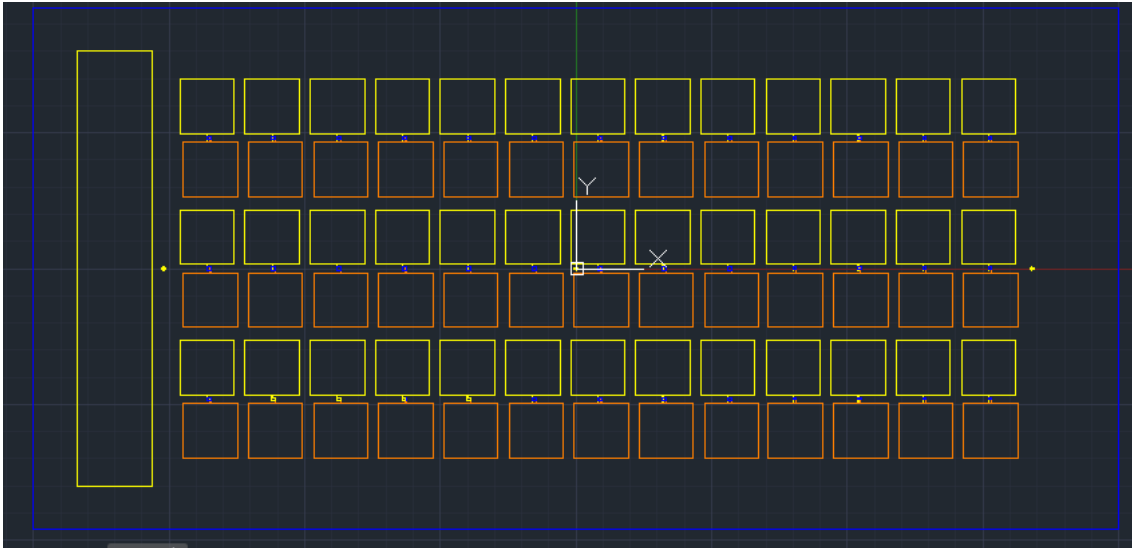


Figure 3: Schematic of the lithography masks used in the fabrication of the micro-heterostructures. The yellow mask represents the metal contacts addressing the bottom graphene layers and a reference mass, the blue mask represents the heterostructures, and the orange mask represents the metal contacts addressing the top graphene layers

-WP1.2.2. Processes for fabrication

The manual stacking of 2D materials as done by multiple **polymer assisted wet transfers of 2D materials**, a staple process in all devices implemented⁹. A layer of low molecular weight PMMA is deposited over the graphene or hBN layer by spin coating, and the opposite side of the copper foil which holds the sample is cleaned of 2D material residues with an oxygen plasma. To release the PMMA and graphene or PMMA and hBN layer, the copper foil is etched at room temperature in 0.5 M FeCl₃ for approximately 3 hours. This resulting membrane is then transferred to a low concentration (2%) HCl for 1 hour and 30 minutes to remove and FeCl₃ residues from the 2DM's surface. After letting the sample rest for 10 minutes in a pure water bath, it is finally transferred to a glass coverslip and dried on a hotplate at 65 °C for 30 minutes. The removal of the PMMA is done overnight in an acetone bath. To finalize the transfer the samples is immersed in IPA and water to remove acetone residues.

The samples requiring microfabrication were assemble by combining the 2DM transfer process with **standard cleanroom processes** such as direct laser writing, spin coating, metal sputtering, and reactive ion etching.

To fabricate the bottom metal contacts, 1035 nm of AZ1505 positive photoresist were spin coated onto a HDMS primed glass coverslip. Direct laser writing was then used to pattern the bottom contact design on the photoresist, which was then developed using AZ400K. A metal stack of Cr/Au (3/10 nm) was deposited via magnetron sputtering, and the contacts were formed by liftoff in an acetone bath with ultrasounds. The 2D material heterostructure stack as then transferred using the same polymer assisted wet transfer method. Another lithography exposure was done to pattern etch protection masks over the heterostruture region and the surrounding 2DM was etched using inductively coupled oxygen plasma. Finally another lithography cycle was done to form the top metal contacts by repeating the steps for the bottom contacts, except the final liftoff was done without ultrasounds, to avoid damaging the graphene and hBN.

The micro heterostructure devices were fabricated using the same process, with the exception of an additional graphene patterning to form the gold/ hBN/ graphene devices, and the top contact lithography was performed using a LOR + AZ1505 photo resist (500 nm/1035 nm) and a mr-Rem 500 solvent at 65 °C for the liftoff.

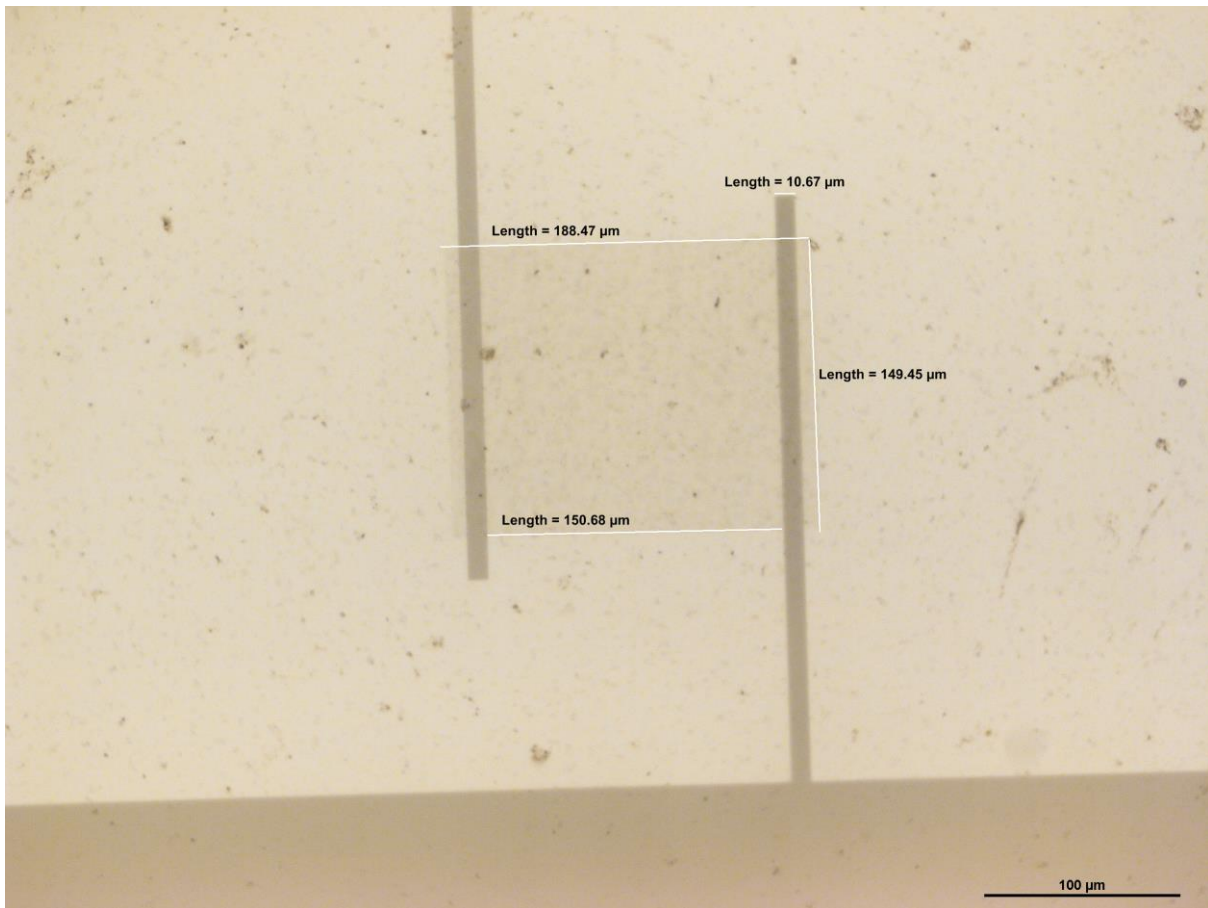


Figure 4: Example of a micro-fabricated graphene/hBN/graphene heterostructure with device area of 150 by 150 μm^2 . The area surrounding the heterostructure is dirtied by debris formed during the 2D material etching step.

In conclusion, while all three of the strategies failed at producing a usable device, all lot of knowledge on how to proceed and handle the 2D materials for future device designs was obtained. With the first strategy it became evident that it was going to be impossible to achieve some preliminary measurements without any microfabrication. The second strategy revealed that the irregularity of the manual 2D material transfer method paired with large heterostructure sizes would result short-circuited devices, due to tearing in the insulator material and the higher likelihood of current transmission through pinholes in the material. The third strategy showed that even with shorter areas the thinness of the hBN layer would render the application of sufficient voltage difference to the graphene impossible without breaking down the material and short-circuiting the device.

Despite all the process sequences failing at producing functioning devices, this can be mainly attribute to the manual handling of the 2D materials, clipping of the material at

the contact edges, and thinness of the hBN layer¹⁰. The standard cleanroom techniques were successfully implemented in the patterning of the 2D material heterostructure and forming metal contacts to electrically address the graphene patches. This part of the work plan is still in its early stages, which is in line with the intended time frame for the task (First 8 to 24 months).

WP2: Graphene and hBN Material characterization

-WP2.1. Morphological characterization

To **characterize the graphene flake morphology**, the samples were heated at 80 ° for 1 to 5 minutes to oxidize the copper foils substrate. Since substrate areas covered in graphene area protected from oxidation, this yields a very noticeable contrast between the graphene and the substrate¹¹. Flake shape and size are then observed on the optical microscope.

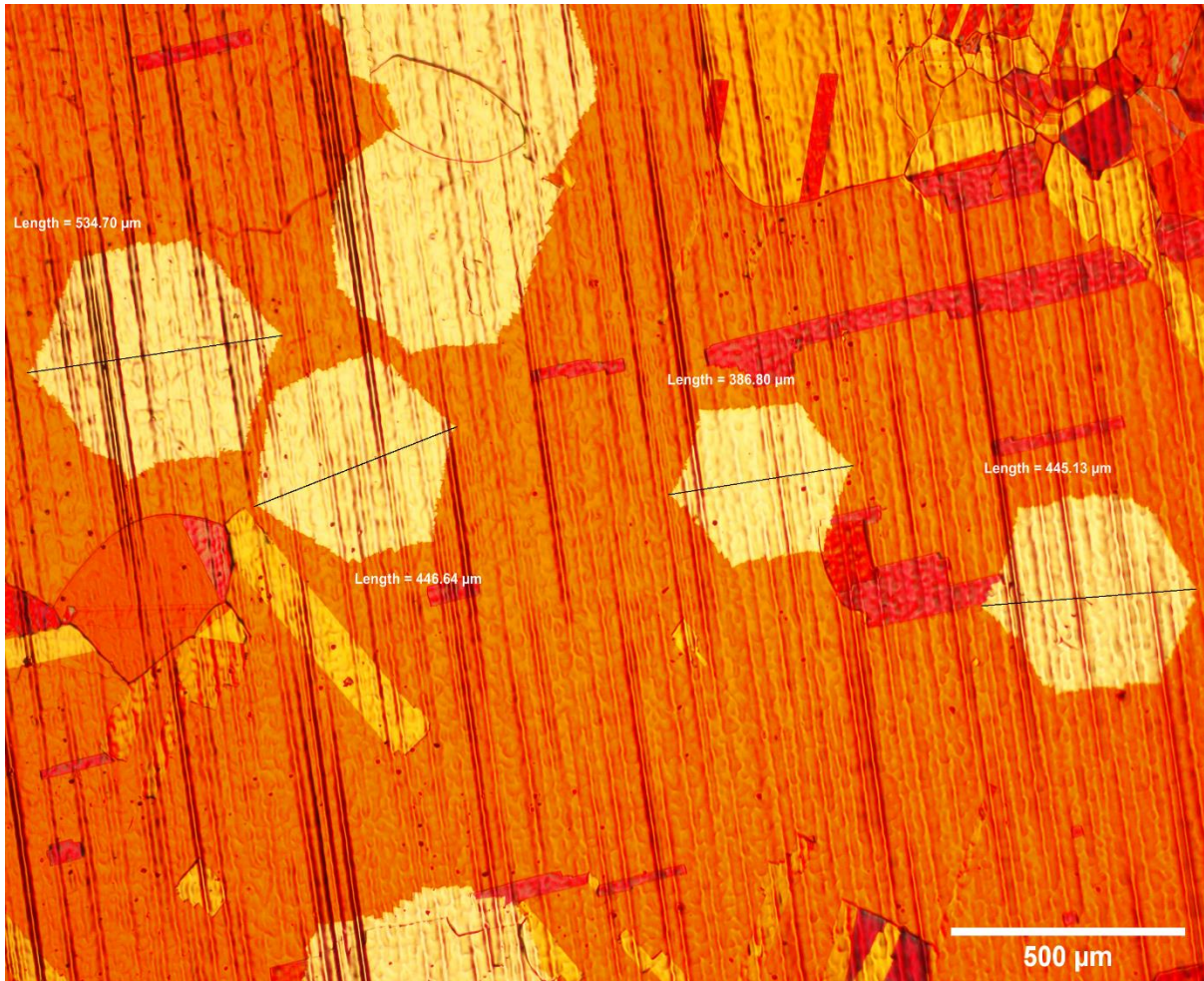


Figure 5: Optical microscope inspection of graphene flakes on copper foil.

that debris is formed during the ICP oxygen plasma etching of the 2DM material stack (see Figure 4). This is a potential indicator that the reaction of oxygen with the 2DMs is originating solid by-products, such as B_2O_3 ¹², rather than easily vented gaseous ones.

Atomic force microscope (AFM) was also performed by a collaborator (João Rodrigues) which determined that the hBN thickness ranges from **2 to 4 nm** and that on the border of the samples small nanoscopic silicon oxide particles are being formed due to sublimation of the quartz reaction tube.

In conclusion, a LP-CVD process was successfully optimized for the fabrication of large single crystal graphene flakes and large grain continuous graphene films in relatively short growth time frames (30 min to 2 hours). A potential issue was also identified in the silicate formation in the hBN, which may interfere in the fabrication and optical characterization of devices.

-WP2.2. Material quality characterization

Raman spectroscopy was performed using a Witec Alpha 300R confocal microscope Raman system to evaluate the monolayer nature and overall material quality of the CVD grown 2D materials and to check the completeness of the 2D material etching steps during the heterostructure microfabrication processes. Excitation was carried out utilizing a Nd:YAG laser of wavelength 532 nm at 2.51 mW power. The signal collection was done using an objective of x50 magnification and 0.7 NA, and the detection was done using a 600 gratings/mm monochromator and UHTS300 spectrometers coupled to the Andor Peltier cooled CCD detectors.

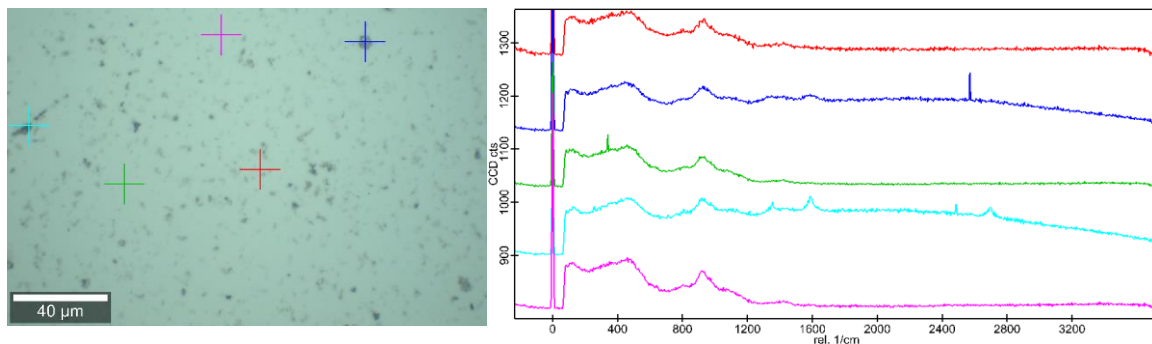


Figure 6: Optical microscope image of the debris produced during the etching of the 2D material stack in the heterostructure microfabrication process (left) and spectra found in the region, colour coded to correspond to the coloured crosses in the optical microscope image. An objective of magnification 50 was utilized.

Figure 6 confirms that, although there is carbon debris remaining on the sample's surface (dark blue and cyan spectra), the oxygen plasma etching process was successful at removing the material for the purposes of patterning the heterostructure.

In conclusion, the oxygen plasma process mentioned in the device processes ([WP1.2.2.](#)) is producing carbon debris and, although for the purposes of electrically modulating the graphene's Fermi level this etching technique suffices, it creates visual clutter that may interfere with the optical measurements. The characterization of material quality was also executed within the intended timeframe (First 8 months).

-WP2.3. Single emitter characterization using Widefield TIRF Microscopy

A Nikon Ti-E widefield **total internal reflection fluorescence (TIRF) microscope** was used to localize and probe SPE brightness over prolonged excitation. Excitation of the hBN colour centres was carried out using different excitation

wavelengths (488, 561, and 647 nm) and different powers to study how the quantum emitters' behaviour changes in function of these parameters, the fluorescence emissions signals were collected using an oil immersion lens of x60 magnification, and recorded using an Andor IXon Ultra 897 EMCCD camera. This technique was also used to compare CVD grown hBN with liquid phased exfoliated (LPE) hBN.

Widefield TIRF measurements, which consisted of 2 minute long recordings with integration time of 50 ms per frame, were collected on hBN samples in areas of 138.24 by 138.24 μm^2 . For 4 of these areas, smaller regions of interest of 34.56 by 34.56 μm^2 were selected within the most focused part of the recordings to ensure that all SPEs in the analysed area are accounted for. Values for the surface density of emitters, intensity time traces, and statistics for fluorescence intermittency events in hBN were extracted using the image processing methodologies explained in WP3.

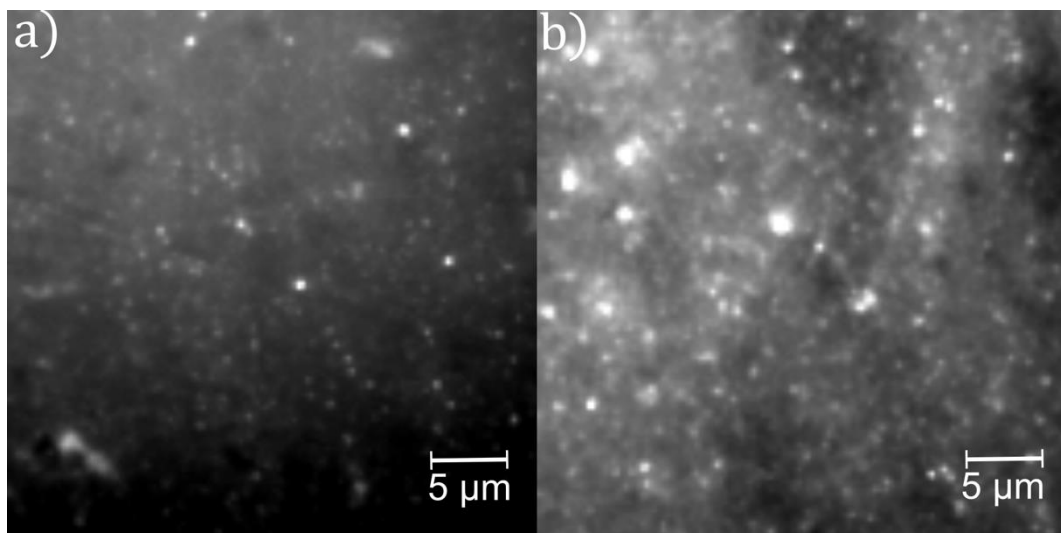


Figure 7: TIRF microscopy images of SPEs in CVD grown hBN (a) and drop cast LPE hBN (b).

In conclusion, single photon emitters were successfully located and their fluorescence signal was recorded using widefield TIRFM, in accordance to the work plan (First 8 months). Fluorescence intermittency behaviours and data sets with pertinent information on SPE properties were recorded at different excitation conditions.

[-WP2.4. Single emitter characterization using lambda mode confocal fluorescence Microscopy](#)

A Zeiss LSM 780 confocal microscope, equipped with a 32 channel GaAsP detector for spectral imaging was used. An oil immersion objective of NA 1.4 and

magnification 63x was used to collect the signal. The spectral detection window across 32 channels of the detector was set to cover an emission wavelength range from 405 to 696 nm, while only the channels covering the range from 520 to 696 nm were considered for the analysis, due to contamination of the remaining channels with scattered laser light. An argon laser's emission line at 488 nm was used to excite the hBN samples at 12.5 mW average power. The 2048 by 2048 pixel hyperspectral confocal fluorescence images (Figure 8) of 32.72 by 32.72 μm^2 CVD grown and drop casted LPE hBN sample areas are formed by scanning the hBN samples with the laser beam and acquiring the signal pixel by pixel with approximately 50 μs integration time and 16 averages per pixel, resulting in a total acquisition time of 1 hour.

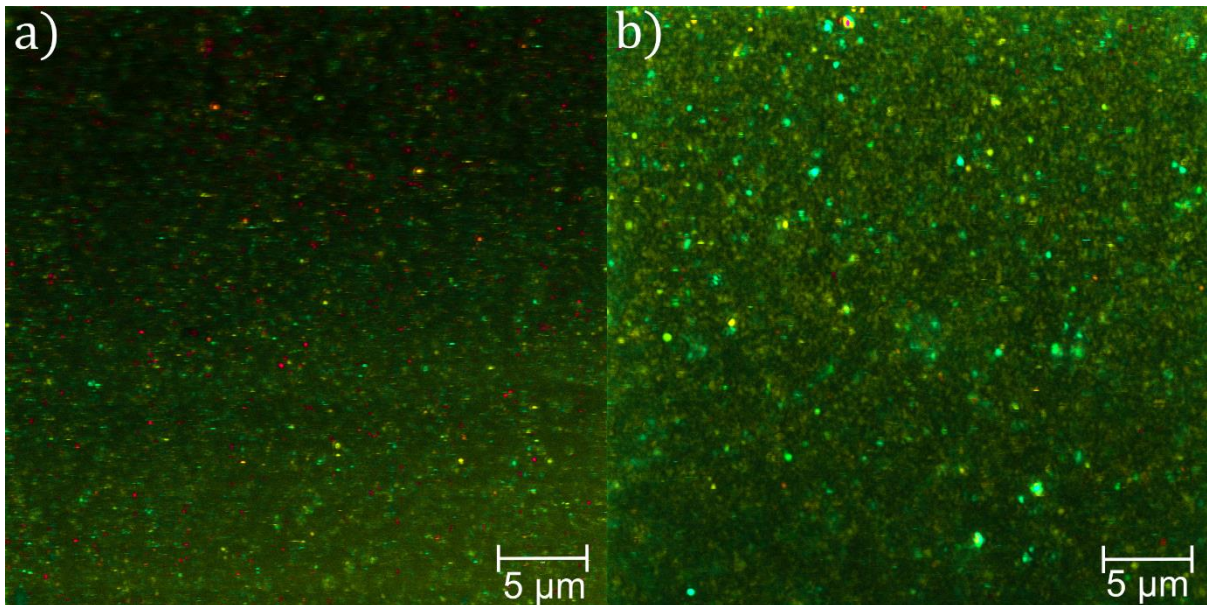


Figure 8: Hyperspectral Fluorescence intensity images of CVD grown (a) and drop casted LPE hBN (b) samples as measured using the Nikon Ti-E wide field TIRF microscope.

In conclusion, very rich data sets containing information on the spectral characteristics of hBN SPEs for two types of hBN sample preparation were gathered, enabling detailed analysis of the emission properties using in-house designed methodologies. This activity was accomplished within the workplan's intended date of the first 12 months of PhD. A potential improvement on this analysis would be to utilize a higher spectral resolution technique

[WP3: Development of new methodologies for SPE data analysis](#)

-WP3.1. Protocols for analysis of Widefield TIRF recordings.

For image processing the **ThunderSTORM plugin in ImageJ** was used to localize intensity spots of the size of the PSF to extract locations of single photon emitters across different areas of the samples recorded using the wide field TIRF setup. From the resulting coordinates table, we filter out the emitters whose standard deviation of detection by the fitting process exceeds 50 nm, to ensure that the emitters are being accurately selected. A table of intensity values over time for each detected emitter is extracted using ImageJ and analysed using custom **MATLAB scripts** which plotted the intensity time trace of the emitters.

From the careful observation of hBN SPEs' time traces it became apparent that **hBN is a very rich system in terms of fluorescence intermittency behaviours**^{13,14}, since a total of 4 distinct behaviours were identified (Figure 9). Two of these intermittency behaviours were labelled as high intensity and low intensity photo-stable (**High PS and Low PS**), since they actually displayed no intermittency and only very small intensity fluctuations, but differed in mean intensity value. Another intermittency behaviour as labelled as spiking (**Spikes**), where mostly stable SPEs would occasionally produce very bright spikes in intensity. Lastly, the most noticeable flickering behaviour was labelled as **wavy or step** due to the clear sinus or square wave intensity trace shape that shows clear transitions between dark and bright emitter states.

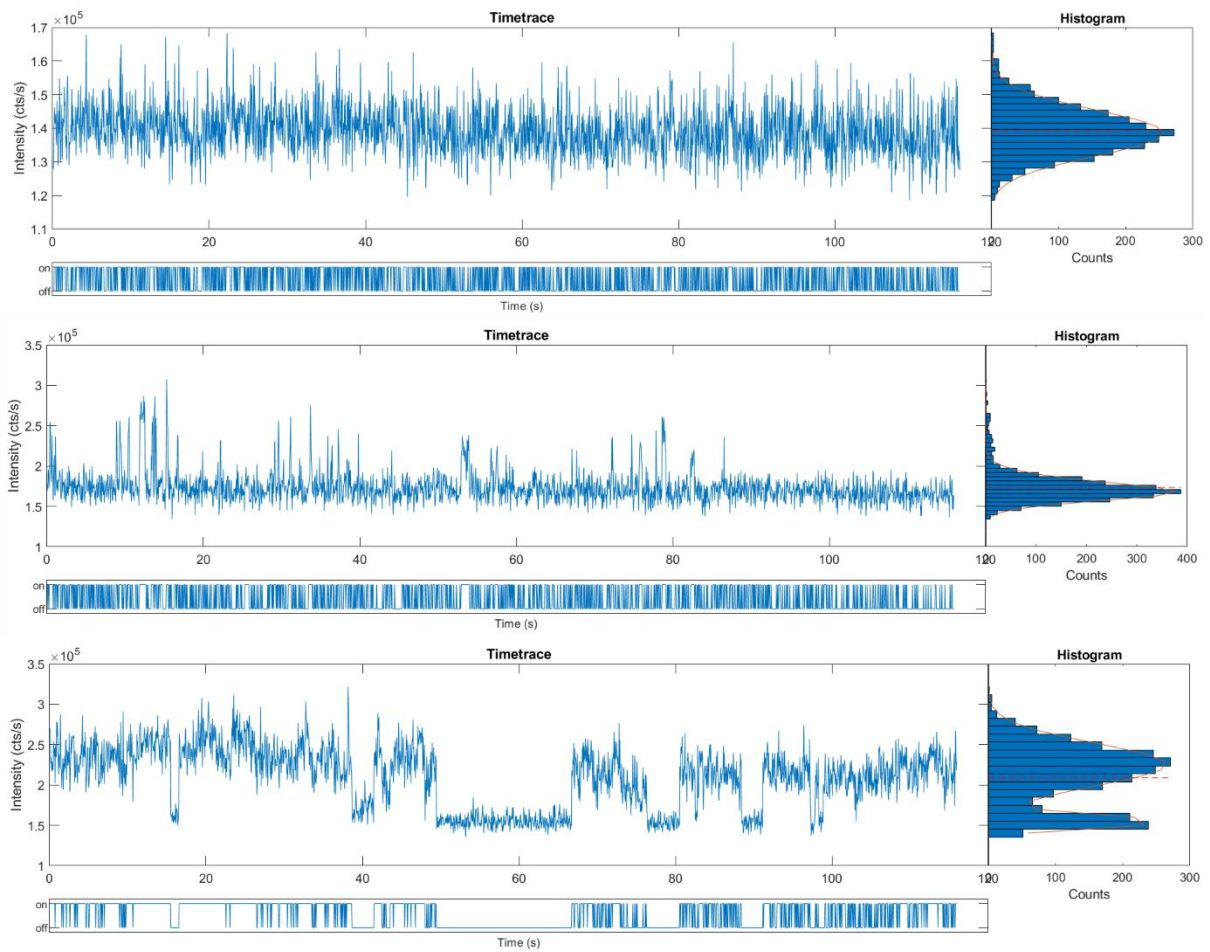


Figure 9: Examples of hBN SPE categories based on fluorescence intermittency behaviour. Low intensity photo-stable (top), Spikes (middle), Wavy or Step (bottom). The intensity distribution histograms and Bright/Dark binary time trace bars are also included.

Several iterations of a custom MATLAB script for the automatic classification of the SPEs in accordance with their type of intensity time trace were implemented. The final and most reliable version of the script follows the ensuing algorithm:

For each detected emitter a histogram distribution is made by binning the recorded intensity values in accordance to Scott's law. To determine a threshold value which separates the dark and bright states' intensities, a weighted average is performed using the histogram distribution, such that the bin values with a larger number of counts are favoured. Because the distribution of intensities follows either a Gaussian pattern or a sum of two Gaussian patterns, when the Bright and Dark states are more easily distinguishable, the weighted average results in either a threshold very central to the Gaussian distribution or a value in between both Gaussians (See histograms in Figure 9). The threshold value, th , is then determined by the expression:

$$th = \sum_i \frac{histo(i)}{sum(histo)} \cdot histbin(i)$$

Where $histo(i)$ is the number of intensity values in the i -th bucket, $histbin(i)$ is the central intensity value associated with the i -th bucket, and $sum(histo)$ is the total number of recorded intensity values for a give trace.

A binary time trace of Bright and Dark states can now be determined by thresholding the intensity time trace. The following step is to count the time duration of the Bright and Dark state time intervals using the binary time trace. It was clear that the **variance of these time duration values was a good distinguishing factor between photo-stable and intermittent emitters**, since intensity fluctuations in stable emitters are always in the order of up to a few tens of ms and in wavy or step type of emitters they can range from tens of milliseconds to tens of seconds, thus have substantially higher time duration variance.

Using the Bright and Dark state time duration variance, an intensity amplitude limit, and the overall mean intensity over time, the categorization of the SPEs follows these rules: If the time duration variance of the Dark and Bright states exceeds 0.01 then the emitter belongs to the Wavy or Step category, otherwise if the emitter intensity exceeds 1.4 times the mean intensity value or is below 0.6 times the mean intensity value then the emitter belongs in the spikes category, since it is too stable to accuse flickering but still possesses a large intensity amplitude. Lastly, in the event that the previous conditions fail, if the emitter mean intensity surpasses the mean intensity of all emitters in the sample then it belongs in the high intensity photo-stable category, otherwise it belongs in the low intensity photo-stable category.

This algorithm enable the counting of SPEs in a sample per flickering behaviour category, and also the **estimation of emitter density under different excitation parameters**.

In conclusion, image processing tools were optimized to locate SPEs in TIRFM data sets and custom MATLAB scripts were developed to extract useful information to analyse, such as emitter intensity over time. Four categories of hBN SPE behaviour were identified based on fluorescence intermittency and brightness and statistical analysis of the

identified SPEs was carried out in function of excitation wavelength and power. This too was accomplished within its intended time frame, within the first 12 months.

[-WP3.2. Protocols for spectral analysis and extraction of useful data from confocal fluorescence microscopy hyperspectral data sets.](#)

To analyse the data obtained via the confocal fluorescence microscope, the **Zeiss Zen Black 3.0** software was used to extract the signature spectra of hBN SPEs and to perform linear unmixing of the recorded images, breaking down the data into 3 intensity maps associated to SPE spectra found in the samples.

Because the hyperspectral images are formed by scanning the sample from left to right and top to bottom, SPEs that display **fluorescence intermittence behaviours** are displayed in the measurement as dashes, half-circles, or interrupted circles, due to the imaging of the pixels of a given SPE being done non-sequentially, such that there are timeframes where when the emitter is being scanned it is in a dark state. ImageJ was used to segment the linear unmixed channels into SPEs and background via thresholding, and to perform the emitter counting by using the built in automatic particle counting tool, which results in the extraction of a data table containing coordinates and shape descriptor values which can be used to classify SPEs as blinkers and non-blinkers.

Using MATLAB's curve fitting toolbox, Gaussian fits of the SPEs' intensity profiles were performed and compared to the expected point spread function (PSF) of a point source of light as observed by the Zeiss LSM 780 confocal microscope.

Detailed analysis of the unmixed data was also carried out for selected SPEs to confirm **spectral diffusion behaviours**^{15,16} by using custom MATLAB scripts. The same area from the centre of the same SPE's PSF was selected in linear unmixed intensity maps corresponding to different spectra and, since pixel dwell is the same for all pixels during the measurement, a timestamp was attributed to each pixel such that a pseudo-time intensity trace corresponding to one each of the spectra could be plotted. Comparing the pseudo-time traces for anti-correlations can reveal the spectral diffusion behaviour.

In conclusion, custom MATLAB scripts in conjunction with ImageJ and Zeiss Zen 3.0 were used to perform image processing on hyperspectral data sets acquired by laser scanning confocal fluorescence microscopy to perform a detailed study of the optical

properties of hBN SPEs, such as emission spectra, fluorescence intermittency, and spectral diffusion. The time frame for the task's completion was within the first 12 months and it was met.

Results

-Graphene properties

A myriad of parameters were tested in graphene CVD and their respective effects were analysed and noted. It was observed that morphology varied from sharp edged “star” shapes to circular graphene blobs, and recipe optimization enabled expansion of flake size from approximately **200 μm to over 1500 μm in diameter**. Recipes were also successfully adapted for continuous graphene film fabrication by adjusting the growth time.

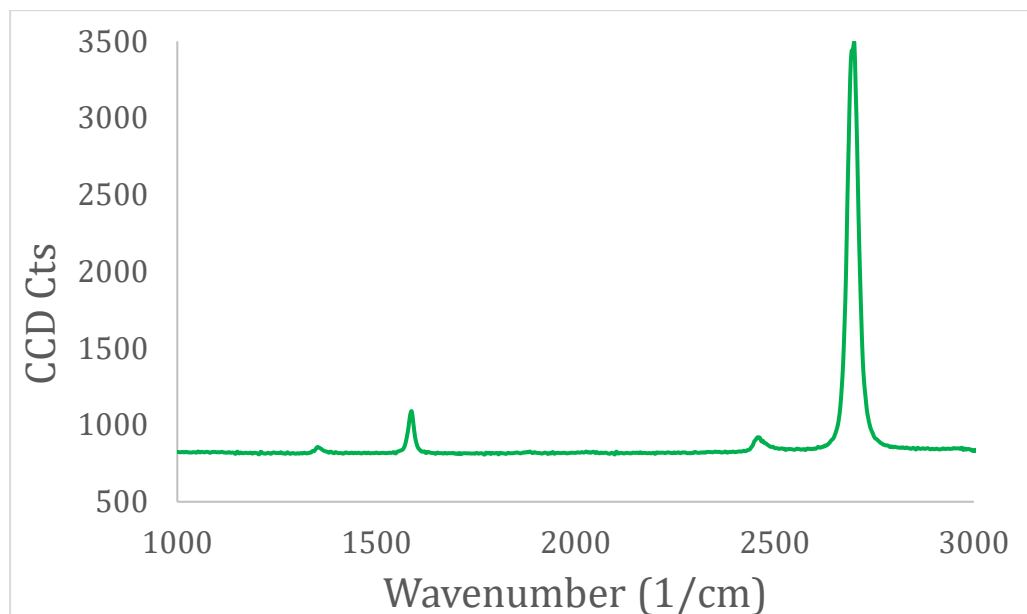


Figure 10: Raman spectrum of a continuous graphene film. Excitation as done using a 532 nm wavelength Nd:YAG laser at 2.51 mW power. Signal was acquired with a 5 s integration time and was averaged 10 times.

Analysing the Raman spectrum for graphene in Figure 10 it is clear that the material is monolayer since the 2D peak ($\sim 2699.9 \text{ cm}^{-1}$), which is characteristic of monolayer graphene, is far larger than twice the G peak (1588.5 cm^{-1}), which is the signature for graphitic materials. Furthermore, the comparatively minuscule D peak

(1351.7 cm^{-1}), which pertains to defects in the graphene's crystal lattice, indicates that the material has **excellent crystallinity**¹⁷.

-Density of defects in hBN

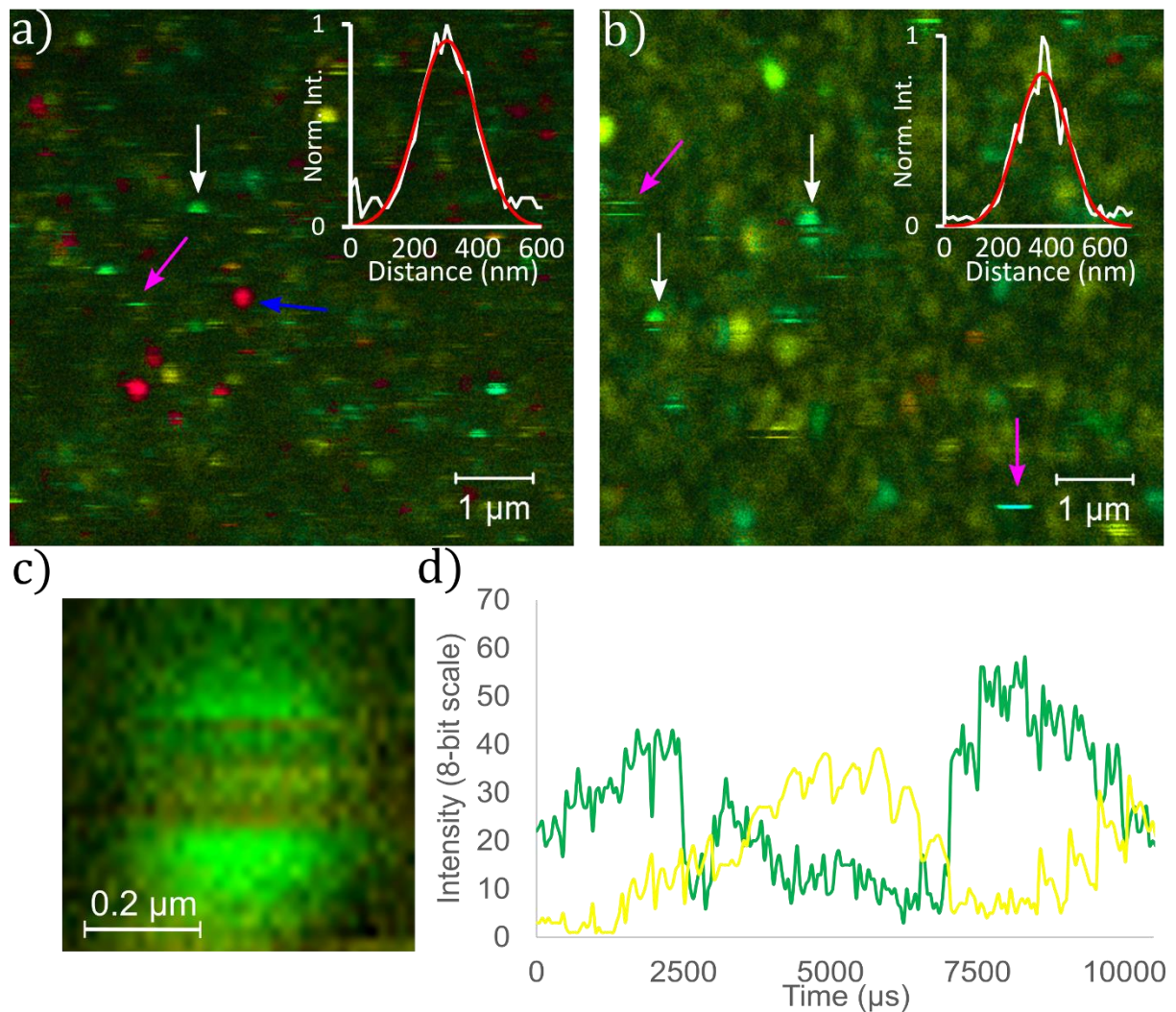


Figure 11: Hyperspectral confocal fluorescence intensity analysis of CVD and drop casted LPE hBN samples. a) Colour-coded fluorescence image of CVD grown sample of hBN. Fluorescence intermittency is manifesting as dashes (indicated by white arrows) or half circles (highlighted by magenta arrows). The inset illustrates the spatial intensity distribution across the emitter highlighted by the blue arrow and the respective Gaussian fit; b) Colour-coded fluorescence image of exfoliated DC hBN. The inset illustrates the intensity profile matching expected PSF, via added Gaussian curve; c) Example of an intensity spot with SPE signature in the drop casted LPE hBN sample, which besides fluorescence intensity intermittency shows spectral emission changes over time; d) Intensity pseudo time trace across the intensity data associated to the single PSF sized area shown in c). The green curve represents the relative contribution from the linear unmixed image associated to spectral component 1 with main peak at 538 nm, while the yellow curve represents the relative contribution to the overall intensity by a different spectral component 2 with main peak at 565 nm.

Single photon emitter (SPE) signatures can be observed in confocal fluorescence intensity images (Figure 11 a and b). The intensity spot shapes largely match the point spread function (PSF) of the microscope (see Figure insets). The PSF for a 488 nm laser and a microscope objective of magnification 63x used with an NA of 1.4 is 220.4 nm and the order of magnitude was verified by performing Gaussian fittings to the intensity profiles, resulting in widths of 217.8 nm and 222.5 nm for CVD and drop cast (DC) hBN material, respectively.

We analysed the single emitter density by determining the **number of SPEs visible in CVD grown and exfoliated hBN samples per unit area**. In the confocal image scans performed over areas of 33.72 by 33.72 μm^2 the density is **$0.675 \pm 0.153 \mu\text{m}^{-2}$** and **$0.230 \pm 0.047 \mu\text{m}^{-2}$** for CVD and DC samples, respectively. Additionally, a faster imaging technique was used to inspect the samples, which may result in slightly different numbers per area due to less integration time per image and thus less laser power/bleaching effects. From images recorded in shorter time (50 ms versus 61 minutes) on this widefield TIRFM system we extract that both the AP-CVD prepared hBN sample and the drop cast LPE hBN sample have similar emitter densities of **$0.095 \pm 0.012 \mu\text{m}^{-2}$** and **$0.134 \pm 0.024 \mu\text{m}^{-2}$** , respectively.

The mean distance between emitters is $3.25 \pm 0.21 \mu\text{m}$ for the CVD grown hBN sample and of $2.73 \pm 0.27 \mu\text{m}$ for the LPE hBN sample as visible in the widefield TIRF images (see Figure 7).

Reported SPE surface density in CVD grown samples varies significantly, with some groups reporting densities as low as 0.04 emitters/ μm^2 ¹³ to higher values such as 2.2 emitters/ μm^2 ¹⁸. In contrast, our CVD grown hBN stands in between with a density of 0.095 ± 0.012 emitters/ μm^2 , which we believe can be an **advantageous characteristic**¹⁹ in terms of making our hBN a good host material for producing large amounts of devices per unit area whilst lessening the difficulty of ensuring that only isolated emitters are used in device fabrication.

[-Advanced hBN SPE spectra characteristics and intermittency behaviour](#)

The data recorded on the confocal microscope further contains spectral information. We analyse the spectral fingerprints, of which there are several as seen in literature^{20,21}, associated to the pixels of the image and **perform a linear spectral unmixing** of the data set using 3 spectral categories for each of the CVD and exfoliated samples, respectively (Figure 11). The colour of the images (Figure 11 a and b) reflects the spectral composition of the fluorescence emission detected across the CVD and DC samples, with additive spectral colour mixture across the detection range (520 to 696 nm).

At some few positions in the image intensity spots with different emission spectra are located in the same area of the PSF, either caused by two defects so close that they are not spatially distinguished with the confocal diffraction limited spatial resolution of the microscope or if both 'colours' blink at the same time - it would indicate that **a single centre would be able to undergo large spectral changes in time**, as indicated by the anti-correlation revealed in the pseudo-time trace between two spectral components of the drop cast, an effect that has been previously observed. The pseudo-time trace of component 1 represented as the green curve in Figure 11 (d) refers to the spectral component of maximum of emission at wavelength of 538 nm, and the pseudo-time trace of component 2 refers to the component of maximum of emission at wavelength of 565 nm is represented by the yellow curve. The respective spectra are shown in Figure 12 (b).

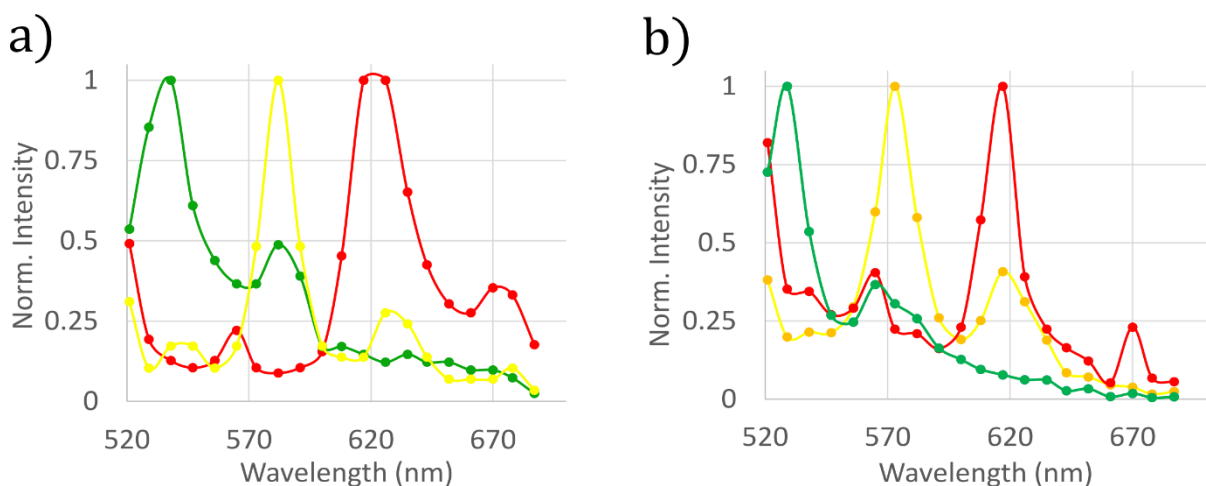


Figure 12: Spectral components isolated from the fluorescence confocal microscopy measurements. Image a) refers to the components selected in the CVD grown hBN sample and b) to the drop casted PLE hBN sample.

The linear unmixing can help us identify the different emitter types that can be excited with a 488 nm laser either via the excitation of the electronic transition or via absorption in higher lying e.g. vibrational bands, resulting in large Stokes shifts, and emission peak maxima positions positioned as far apart from the excitation wavelength at **538, 591, and 617 nm** for the representative emission spectra observed for emitters in AP- CVD grown samples (see Figure 12 a) the green , yellow and red spectra , and at **538, 565, and 617 nm** for the representative emission spectra observed for emitters in drop cast LPE samples, respectively.

The energy differences between the associated high intensity emission peaks and the lower energy peak apparent as a red shifted shoulder, have been determined to be 0.175 eV , 0.150 eV and 0.159 eV for AP-CVD recorded spectra with emission peak maxima at 538 , 591, and 617 nm and to be separated by 0.150 eV, 0.155 eV , 0.159 eV and 0.159 eV in case of exfoliated hBN samples for spectra recorded with emission peak maxima at 529 nm , 565 nm and 617 nm, respectively.

Intermittent blinking processes manifest themselves as deviations from circular intensity spot patterns in the fluorescence intensity images recorded by laser scanning confocal imaging, which was performed from the top to the bottom and from left to right across the characterized sample area.

The blinking associated deviations from circular shapes include, intensity spots in the shape of half circles (highlighted by white arrows), single lines or stripes (highlighted by magenta arrows).

Analysis of SPE statistics based on their spectra revealed that 28.42% of the SPEs in our AP-CVD hBN have a 538 nm intensity peak maximum signature, 25.82% have their peak intensity at 591 nm, and 47.76% have their maximum at 617 nm, whereas in the drop cast LPE sample these statistics are 36.05%, 42.29%, and 21.66% for spectral signatures with emission peak maxima at 529 nm, 565 nm and 617 nm, respectively. Spot shape analysis also enabled the extraction of SPE statistics based on fluorescence intermittency behaviour, which indicate that for the AP-CVD hBN 18.67% and 81.33% of emitters are, respectively, non-intermittent and intermittent, and likewise for the LPE hBN 26.86% and 73.14% of emitters are, respectively, non-intermittent and intermittent.

An intensive study of TIRF data gathered on AP-CVD hBN SPEs yielded the following results for the different categories established at different wavelengths and powers of excitation. For the **high intensity photo-stable emitters** it became apparent that for higher excitation power the density of this calls of emitter rises, indicating that higher excitation power may be a requirement for stable non-intermittent emission. It is also noticeable that this category of SPE is more responsive to the 488, and 561 nm excitation than to the 647 nm excitation (Figure 13).

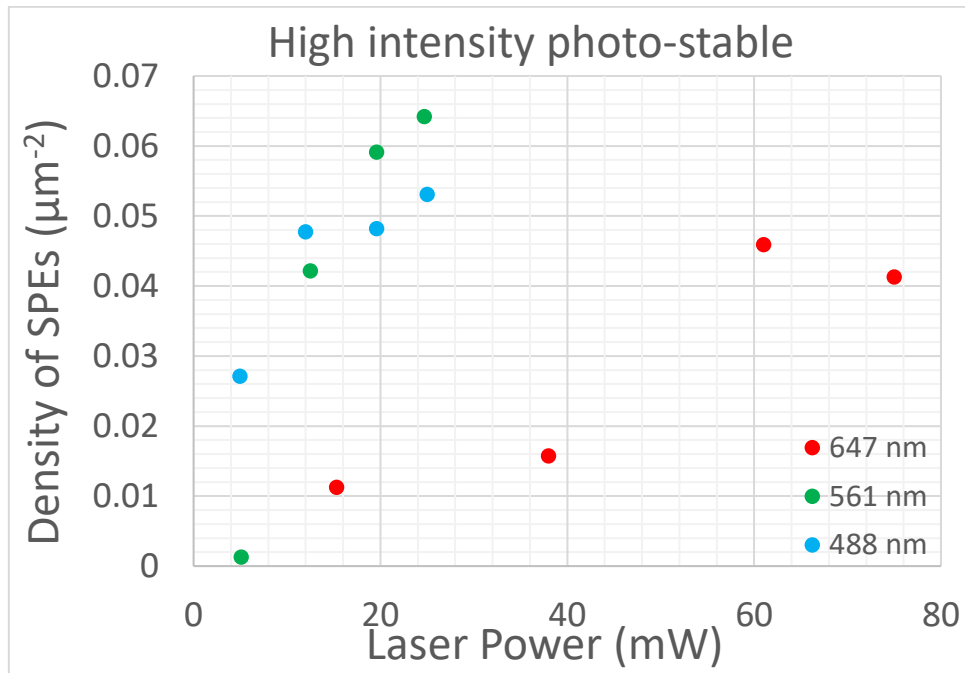


Figure 13: Surface density of high intensity photo-stable SPEs in AP-CVD hBN as determined by the analysis of data sets acquired in the TIRFM setup for different excitation laser powers and wavelengths.

The same behavioural trends as in the **low intensity photo-stable emitters** were observed for their low intensity counterparts, as seen in Figure 14.

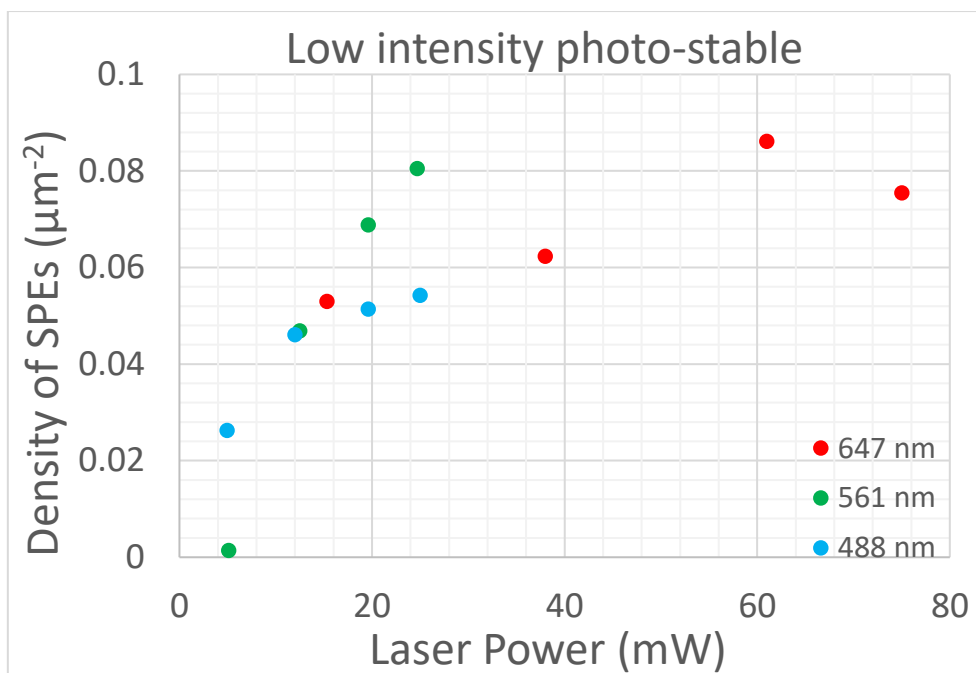


Figure 14: Surface density of low intensity photo-stable SPEs in AP-CVD hBN as determined by the analysis of data sets acquired in the TIRFM setup for different excitation laser powers and wavelengths.

In contrast, the **spikes** category of blinker shows the opposite trend to the stable emitter (Figure 15), where the density of this class decreases to near vanishing degrees with increasing excitation power. It is also notable how this type of emitter is barely activated under 488 nm excitation.

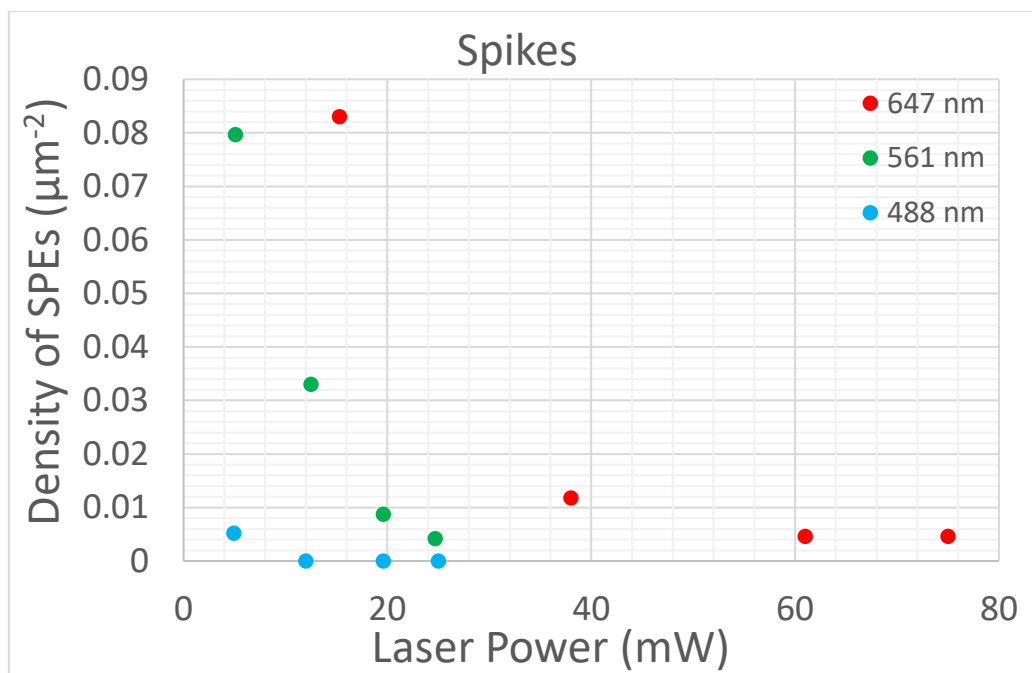


Figure 15: Surface density of spiking SPEs in AP-CVD hBN as determined by the analysis of data sets acquired in the TIRFM setup for different excitation laser powers and wavelengths.

Finally, it was observed that the fluorescence intermittent **wavy or step** category of SPEs were substantially more responsive to 647 nm excitation, and fluctuated with power (Figure 16). The low surface density of intermittent SPEs at 488 nm excitation contrasts heavily with the findings from the analysis of the confocal fluorescence microscope data sets, but since those measurements happen at longer integration times and the signal acquisition is performed pixel per pixel instead of simultaneous image acquisition, as is the case for the TIRFM, we find these results to be more trustworthy.

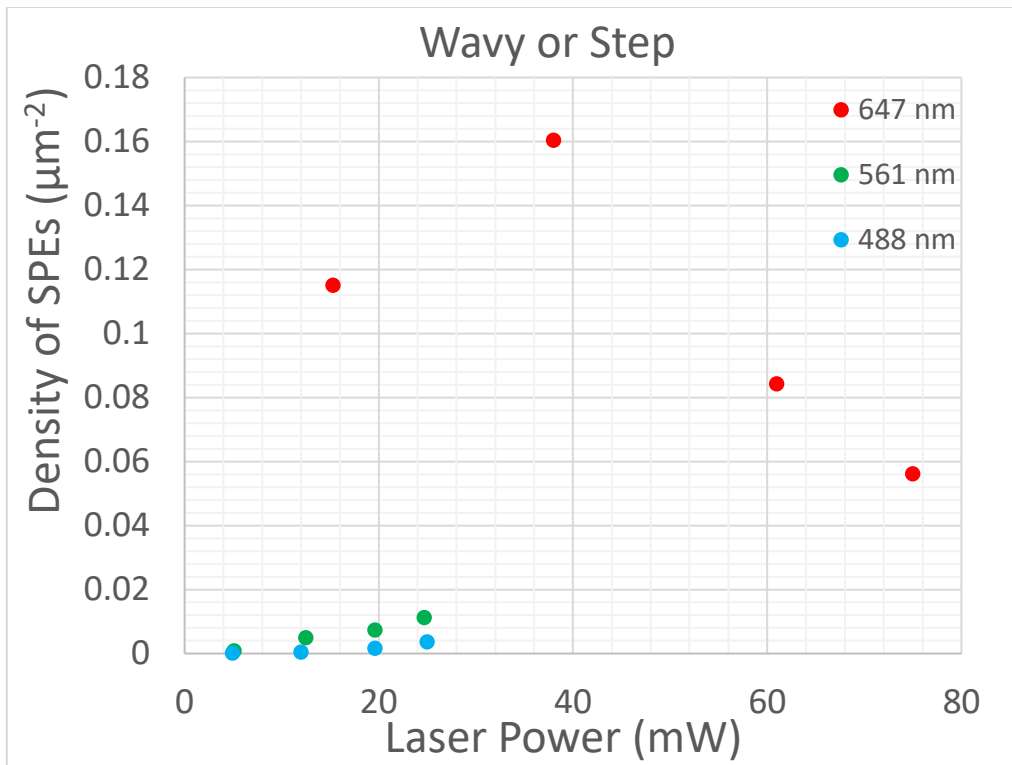


Figure 16: Surface density of wavy or step intermittent SPEs in AP-CVD hBN as determined by the analysis of data sets acquired in the TIRFM setup for different excitation laser powers and wavelengths.

Comparisons of intermittent emitter densities were drawn between AP-CVD hBN and graphene covered AP-CVD hBN to inspect **the effect the presence of graphene** has on the emission characteristics of SPEs.

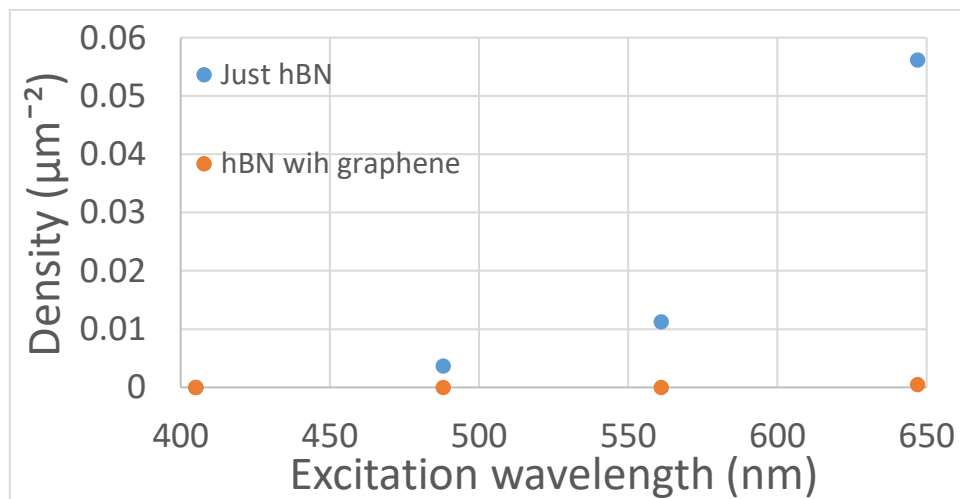


Figure 17: Surface density of fluorescence intermittent wavy or step SPEs in hBN and graphene covered hBN at different wavelengths of excitation at the maximum available powers.

As seen in Figure 17, the addition of graphene to the system produces a passivation effect on the SPEs, resulting in **near total extinguishing of the flickering behaviour**. We attribute this to the redistribution of charge provided by the addition of a metal like layer such as graphene, since the SPEs are environmentally sensitive, this result indicates that the fluorescence intermittency is mediated by local charge fluctuations in the vicinity of the crystal defects.

Conclusions:

The student successfully completed the curricular component of the MAPfis physics doctoral programme in which he is enrolled, gaining knowledge foundations in the advanced physics topics of nano-optics, advanced material preparation and characterization, single photon sources in photonics devices for quantum technologies, and physics of electronics materials and devices;

Three strategies for early prototyping of the PhD's target device were attempted and allowed for valuable information for the implementation of future designs to be obtained;

Most planned deliverables, as was the case for reports on material characterization and on hBN SPE surface density, were met, with the exception of the Hanbury-Brown-Twiss experiment for the confirmation of the quantum mechanical nature of the hBN single photon emitter, as part of WP3 (to be done soon as of the time of the writing of this report). Additional work parallel to the scope of the PhD was done, such as LPE hBN characterization and detailed study statistical analysis of hBN SPEs' fluorescence intermittency behaviour.

Large graphene flakes and graphene films of excellent crystallinity were successfully fabricated and characterized, and methods for 2-4 nm hBN CVD growth containing SPE densities of $0.095 \pm 0.012 \mu\text{m}^{-2}$ were also developed. Additionally LPE hBN samples were prepared by drop casting, analysed, and compared to the hBN CVD samples.

The SPE signatures were obtained via confocal fluorescence microscopy and labelled in accordance to their emission peak maxima of **538, 591, and 617 nm** for the CD hBN sample and **538, 565, and 617 nm** for the LPE drop cast hBN sample. Large spectral changes were also observed in some selected SPEs and an anti-correlation between linear unmixed intensity maps associated to different spectra was analysed to verify this spectral diffusion behaviour.

Statistical analysis of SPEs based on fluorescence intermittency behaviour, of which 4 categories of SPE were identified, was carried out for both TIRFM and confocal fluorescence microscopy data sets, and, in specific for the TIRFM datasets, the effects of excitation power and wavelength on these statistics were studied. This study revealed that SPEs tend to have large densities of stable emitters for higher excitation power across all considered wavelengths and that the high intensity photo-stable emitters are most responsive to 561 nm excitation wavelength. The spiking behaviour decreases to near vanishing degrees with increasing power and is particularly uncommon under 488 nm excitation. Finally the wavy or step SPEs are most common under 647 nm excitation.

To check how the graphene affects the hBN quantum emitters, TIRFM data sets of graphene covered hBN samples were analysed and the resulting statistics were compared to the statistics of AP-CVD hBN, revealing that the graphene addition results in an almost complete extinguishing of the fluorescence behaviour, most likely due to a passivation effect of local accumulated electric charges in the vicinity of the flickering SPEs, who are environment sensitive²².

[Collaborations](#)

Several collaborations were established to accomplish the report work and also to contribute to other work outside the scope of the PhD. The main collaborators were the following:

-Andrea Cappasso (INL), who provided a dispersion of LPE hBN in IPA for the drop cast comparisons;

-João Freitas (INL and U. Minho), received support in data analysis of TIRFM data sets pertaining to the study of DNA hybridization kinetics on the single-molecule level using graphene near-field effects;

-João Rodrigues (INL), performed AFM measurements of AP-CVD hBN samples;

-João Fernandes (U. Minho and INL), provided some AP-CVD hBN samples;

-Prof. Axel Lorke (U. Duisburg Essen), who agree to host the student at U. Duisburg Essen for cryogenic temperature measurements of hBN SPE spectral properties;

- Graphene RF devices group (U. Bristol), who agree to support the student in the fabrication of active electric matrices for the electrical addressing of many nanoscopic 2D material heterostructures;

-Jerôme Borme (INL), who gave advice and consultation on the organization and drafting of the microfabrication process flows;

-Prof. Ricardo Ribeiro (INL and U. Minho), Opened discussion on performing theoretical analysis and simulations of hBN SPEs based on the experimental data.

Dissemination

The student's efforts contributed to the following publications and presentations at conferences:

- NanoPT2020, NanoPT2020, online conference, September 23-24, 2020 Sept 2020: Poster Oxygen assisted monocrystalline graphene growth by chemical vapor deposition Oxygen assisted monocrystalline graphene growth by chemical vapor deposition, Vitor Silva, Tiago Queirós, Ivo Colmiais, George Junior, Chun-Da Liao, Pedro Alpuim.

- FOM2021, Kinetics of DNA hybridization observed on single molecule level using Graphene nearfield effects João Carlos Roberto de Freitas, Tiago Queirós, Agnes Purwidyantri, Pedro Alpuim, Jana B. Nieder.

Participation in seminars and conferences:

The student attended the following seminars and conferences:

- CarbOnlineHagen 2020-Graphene growth and Carbon technologies (8 40 minute seminars);
- Technology Unites Global summit- MEMS & Imaging Sensors Forum (3h session);
- QPI Lectures- Pascale Senellart/ Pablo Jarillo-Herrero (2 1 hour Seminars);
- Flashtalk at INL symposium 2020 (ranked in the top 4 best presentations);

The student also contributed to scientific outreach activities:

- UPA Digital, Presenting Engineering Physics to secondary school students (2020/2021 Wed 5/05, 15:30-16:30).

References:

1. Aharonovich I, Englund D, Toth M. Solid-state single-photon emitters. *Nat Photonics*. 2016;10(10):631-641. doi:10.1038/nphoton.2016.186
2. Lee H, Paeng K, Kim IS. A review of doping modulation in graphene. *Synth Met*. 2018;244(March):36-47. doi:10.1016/j.synthmet.2018.07.001
3. Li W, Chen B, Meng C, et al. Ultrafast all-optical graphene modulator. *Nano Lett*. 2014;14(2):955-959. doi:10.1021/nl404356t
4. Zhao X, Li L, Zhao M. Lattice match and lattice mismatch models of graphene on hexagonal boron nitride from first principles. *J Phys Condens Matter*. 2014;26(9). doi:10.1088/0953-8984/26/9/095002
5. Grosso G, Moon H, Lienhard B, et al. Tunable and high-purity room temperature single-photon emission from atomic defects in hexagonal boron nitride. *Nat Commun*. 2017;8(1):1-8. doi:10.1038/s41467-017-00810-2
6. Wrachtrup J. 2D materials: Single photons at room temperature. *Nat Nanotechnol*.

- 2016;11(1):7-8. doi:10.1038/nnano.2015.265
7. Ruiz I, Wang W, George A, Ozkan CS, Ozkan M. Silicon Oxide Contamination of Graphene Sheets Synthesized on Copper Substrates via Chemical Vapor Deposition. *Adv Sci Eng Med*. 2014;6(10):1070-1075. doi:10.1166/ asem.2014.1615
 8. Cho SY, Kim MS, Kim M, et al. Self-assembly and continuous growth of hexagonal graphene flakes on liquid Cu. *Nanoscale*. 2015;7(30):12820-12827. doi:10.1039/c5nr03352g
 9. Backes C, Abdelkader AM, Alonso C, et al. Production and processing of graphene and related materials. *2D Mater*. 2020;7(2). doi:10.1088/2053-1583/ab1e0a
 10. Nasr Esfahani A, Malcolm AJ, Xu L, et al. Ultra-thin films of solution-exfoliated hexagonal boron nitride by Langmuir deposition. *J Mater Chem C*. 2020;8(39):13695-13704. doi:10.1039/d0tc02933e
 11. Topsakal M, Aahin H, Ciraci S. Graphene coatings: An efficient protection from oxidation. *Phys Rev B - Condens Matter Mater Phys*. 2012;85(15). doi:10.1103/PhysRevB.85.155445
 12. Liu Z, Gong Y, Zhou W, et al. Ultrathin higher-temperature oxidation-resistant coatings of hexagonal boron nitride. *Nat Commun*. 2013;4(May):1-8. doi:10.1038/ncomms3541
 13. Stern HL, Wang R, Fan Y, et al. Spectrally Resolved Photodynamics of Individual Emitters in Large-Area Monolayers of Hexagonal Boron Nitride. *ACS Nano*. 2019;13(4):4538-4547. doi:10.1021/acsnano.9b00274
 14. Koperski M, Nogajewski K, Potemski M. Single photon emitters in boron nitride: More than a supplementary material. *Opt Commun*. 2018;411:158-165. doi:10.1016/j.optcom.2017.10.083
 15. Sontheimer B, Braun M, Nikolay N, Sadzak N, Aharonovich I, Benson O. Photodynamics of quantum emitters in hexagonal boron nitride revealed by low-temperature spectroscopy. *Phys Rev B*. 2017;96(12):1-5. doi:10.1103/PhysRevB.96.121202

16. Li X, Shepard GD, Cupo A, et al. Nonmagnetic Quantum Emitters in Boron Nitride with Ultranarrow and Sideband-Free Emission Spectra. *ACS Nano*. 2017;11(7):6652-6660. doi:10.1021/acsnano.7b00638
17. Malard LM, Pimenta MA, Dresselhaus G, Dresselhaus MS. Raman spectroscopy in graphene. *Phys Rep*. 2009;473(5-6):51-87. doi:10.1016/j.physrep.2009.02.003
18. Mendelson N, Xu ZQ, Tran TT, et al. Engineering and Tuning of Quantum Emitters in Few-Layer Hexagonal Boron Nitride. *ACS Nano*. 2019;13(3):3132-3140. doi:10.1021/acsnano.8b08511
19. Fröch JE, Hwang Y, Kim S, Aharonovich I, Toth M. Photonic Nanostructures from Hexagonal Boron Nitride. *Adv Opt Mater*. 2019;7(4):1-6. doi:10.1002/adom.201801344
20. Li C, Xu ZQ, Mendelson N, Kianinia M, Toth M, Aharonovich I. Purification of single-photon emission from hBN using post-processing treatments. *Nanophotonics*. 2019;8(11):2049-2055. doi:10.1515/nanoph-2019-0099
21. Matthew A. Feldman, Claire E. Marvinney, Alexander A. Puretzky and BJL. Evidence of photochromism in a hexagonal boron nitride single-photon emitter. *Optica*. 2021;8(1):1-5.
22. Mendelson N, Chugh D, Reimers JR, et al. Identifying carbon as the source of visible single-photon emission from hexagonal boron nitride. *Nat Mater*. doi:10.1038/s41563-020-00850-y